Proceedings World Geothermal Congress 2010
Bali, Indonesia, 25-29 April 2010

Microseismicity and 3-D Mapping of an Active Geothermal Field, Kilauea Lower East Rift Zone, Puna, Hawaii

Catherine Lewis Kenedi, Eylon Shalev, Alan Lucas, and Peter Malin

IESE University of Auckland, Private Bag 92019, Auckland 1142, New Zealand

katelk@auckland.ac.nz

Keywords: shear-wave splitting, double difference relocation, seismicity, 3-D tomography, borehole seismometry

ABSTRACT

The local fault and dike structures in Puna, southeastern Hawaii, are of interest both in terms of electricity production and volcanic hazard monitoring. The geothermal power plant at Puna has a 30 MW capacity and is built on a section of the Kilauea Lower East Rift Zone that was resurfaced by lava flows as recently as 1955 and 1960.

The Puna Borehole Network was established in 2006 in order to provide detailed seismic data about the Puna geothermal field. The array consists of eight 3-component borehole seismometers. The instrument depths range from 24 to 210 m (80 to 690 ft); five stations with 2 Hz geophones and three with 4.5 Hz geophones.

The large majority of events were < M0.5 and occurred at depths between 2 and 3 km. The size, location, and depth of the microearthquakes suggest that power plant activity affects local seismicity. Earthquake depths increase from NE to SW, trending up the rift zone towards the Kilauea summit. Depths also increase from the study area to the SE, consistent with active normal faulting along Kilauea's south flank. Shear wave polarization indicates that the active, fluid-filled fracture system trends SW-NE, consistent with the orientation of the LERZ. Double difference relocation suggests an intersecting network of fractures with both NE and approximately NW trends.

3-D tomographic analyses of P-wave velocity, S-wave velocity, and the Vp/Vs ratio are also presented. An area of anomalously fast P-wave velocity at the relatively shallow depth of 2.5 km may be evidence for a dense, gabbroic intrusion. This intrusion may underlie and be the parent of a body of dacitic melt that was discovered under the geothermal field during drilling.

1. INTRODUCTION

The Puna geothermal system is located along the volcanically active Lower East Rift Zone (LERZ) of Kilauea Volcano, on the island of Hawaii, USA. Exploration for geothermal resources on the LERZ started in the 1960's; the geothermal power plant, Puna Geothermal Ventures (PGV), has been operating since 1993. The 30MW field supplies approximately 30% of the electricity needs of the Big Island of Hawaii. By working with PGV, we gained access to this active resource.

The seismicity of the Puna geothermal system has not been well described until now, when a borehole seismic network has allowed us to record small local microearthquakes. At geothermal systems around the world, both natural and induced seismicity have been documented extensively, and the majority of these earthquakes are small. Because the PGV geothermal plant is in a populated and seismically noisy area, borehole instruments reduce the surface noise and are more effective at recording geothermal seismicity. Having recorded and located >4000 microearthquakes, we applied the data to three analytical components: Shear wave splitting, double difference earthquake location, and 3-D tomography.

Shear wave splitting analysis is a widely used means of determining fracture orientation. The method is based on the principal that shear waves polarize into a faster and a slower wave when they encounter aligned fractures (Crampin, 1981). The particle motion of the faster wave generally aligns in the direction of fracture orientation. Fluid saturated fractures in geothermal areas include both micro-faults and macro-faults from which strong shear wave polarization can occur (Crampin, 2005). In the Puna geothermal area, the major fluid conduits appear to be large fractures, making it of great interest to understand their orientation and location. Shear wave splitting has been used successfully in geothermal areas to identify the direction of primary and secondary stress-aligned fractures (e.g. Lou et al., 1997; Tang et al., 2008).

The double difference algorithm of earthquake relocation (Waldhauser and Ellsworth, 2000; Waldhauser, 2001) resolves earthquake locations from a cloud or cluster to a plane or linear feature as would be expected for a fault. The method correlates hypocenters based on P- and S-wave arrival times and/or waveforms correlation and relocates them with respect to other "related" earthquakes. This eliminates the uncertainties associated with the velocity model and picking errors. The method has been used to identify seismogenic structure in both magmatic systems (e.g. Prejean et al., 2002 and 2003) and geothermal systems in trying to resolve "clouds" of earthquakes associated with fluid flow and injection (e.g. Lippitsch et al., 2005; Clarke et al., 2009).

A third method for visualizing the structure of geothermal systems is 3-D seismic tomography. In geothermal areas, methods of tomographic inversion have been used to improve knowledge of local velocity structure (e.g. De Matteis et al., 2008) and have a proposed use to monitor changes in geothermal and magmatic reservoirs (Gunasekera et al., 2003; Chiarabba and Moretti, 2006). The method has been documented extensively with respect to magmatic systems (see the review by Lees, 2007, and references therein), including Kilauea, but has not been applied along the Lower East Rift Zone, nor with the localized focus of our seismic network.

In 3-D tomography, the resolution of the inversion increases with the number of seismic stations; the resolution is determined by the number of raypaths between the hypocenter and the seismic receiver that cross through each volume of a designated 3-D grid. As the number of receivers increases, so does the number of raypaths from the

earthquake; with increasing raypaths, the volumes within the 3-D grid can be decreased and the resolution increases.

In this study we use microseismicity to investigate the fault and fracture system in the Puna geothermal field. We use the locations of >4000 microearthquakes to improve the local velocity model, identify fault and fracture orientations, and use 3-D tomography to locate zones of high and low seismic velocities. Along this segment of the LERZ, water, magmatism, and fractures have coincided to create a permeable, steam-rich, high-temperature environment. The goal of our work is resolving the inner structure of this system.

2. GEOLOGIC CONTEXT

Kilauea Volcano is a long, narrow structure built on the shoulder of the neighboring volcano Mauna Loa; Kilauea has a summit crater, the site of both effusive and explosive volcanism, from which two major rift systems extend. The Puna geothermal field is located on the Lower East Rift Zone (LERZ), approximately 40 km east of the summit. The local geology consists of basalt flows underlain by hyaloclastites and injected by basaltic dikes (Trusdell et al., 1993). Volcanic activity has included fissure eruptions with fountaining and lava flows; the LERZ has been resurfaced by lava flows over the last 300 years (Moore and Trusdell, 1991). The lava flows in the area of the geothermal system are from 1955 (Moore and Trusdell, 1991). This section of the LERZ contains an apparent "jog" in the rift (Figure 1). Two lines of cones and craters extend from this "jog," both oriented SW-NE, but offset by approximately 1.5 km. The geothermal system is within the offset, which is encompassed in the borehole network among stations P02, P01, P03, and P05 (Figure 1).

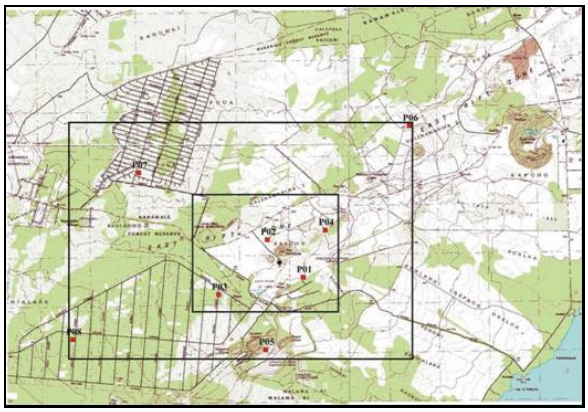

Figure 1: Topographic map of the Puna Borehole Network area. Red squares mark station locations. The black dot is Puna Geothermal Ventures. The large black rectangle is the target zone for the 3-D inversion. The small black rectangle is the area of good ray coverage shown in detail in other 3-D plots.

The most extraordinary geologic aspect of the Puna geothermal field is the confirmed presence of dacitic magma at approximately 2.5 km depth (Marsh, 2008; Teplow, 2008). The magma was discovered during routine drilling at PGV. The drill team inadvertently drilled into active magma, which repeatedly oozed up the well bore while the drill bit was withdrawn and relowered; drilling was stopped when clear glass chips came out as cuttings. The magma demonstrates both the unpredictable nature of this system and, perhaps, an explanation for the local high heat levels. Much work remains in terms of discovering the source of the magma, and we intend our contribution to be towards understanding the structure that encouraged the magma to accumulate and differentiate under the Puna geothermal field.

3. NETWORK SETUP

The Puna Borehole Network consists of eight 3-component seismographs (Figure 2A and 2B) centered on the geothermal field in two concentric rhombs (Figure 1); the design maximizes both coverage for locating earthquakes and angles to calculate shear wave splitting data. Two stations are located at PGV; others are on private property where owners were approached by PGV personnel and kindly agreed to allow us to set up a permanent station. The station depths range from 30 – 210 meters. The instruments have been designed to work in HQ-type boreholes, diameter ~100 mm; seven of the boreholes were drilled for the array, and the eighth hole was an existing water well. The latter (P04) is the deepest and hottest borehole, with a temperature of 90°C.

Figure 2: (2A) = Inside of the 3-component borehole seismometer. Top geophone is vertical; middle and bottom geophones are horizontal and orthogonal. Geophones are the small cylinders; the large conical shapes are gimbaled counterweights to control for borehole tilt and contribute to damping. (2B) = Installation of a seismometer into a standard diameter HQ borehole. Top half of the instrument is a tiltmeter.

Five instruments consist of gimbaled 2 Hz geophones (Figure 2B), whereas the other three instruments (P01, P02 and P04) consist of gimbaled 4.5 Hz geophones. Two of the stations (P01 and P02) also include a tiltmeter and an accelerometer. Acquisition units are Reftek 130 recorders from which data cards are collected and uploaded. Data is continuously recorded at a sampling rate of 200 samples/sec; data cards are collected every 10 days. Following upload, the events are identified by a triggering program and are located using HYPOINVERSE-2000 (Klein, 2002) after P and S arrivals are picked manually.

4. LOCAL SEISMOLOGY

The array has recorded about 6000 earthquakes since June, 2006 (Figure 3). First arrivals were picked by hand then earthquakes were located using HYPOINVERSE-2000 (Klein, 2002). Seismicity occurs in a northeast-trending linear swath consistent with the orientation of the Kilauea Lower East Rift Zone. The majority occurs under the

geothermal plant, at depths from 1.5 to 3.5 km; this is consistent with geothermal production and injection at these depths. Earthquakes at depths of 3.5–5.5 km occur throughout the system but are most visible up-rift towards Kilauea summit. Earthquakes of increasing depth occur to the southeast of the rift; this is consistent with the presence of a large normal fault of northeasterly strike and southeasterly dip. Such a fault has been suggested in field mapping but not described in detail; the presence of the fault would be consistent with the southerly movement of the south flank of Kilauea along the dominant plane underlying the Hilina Fault System (Parfitt, 2001).

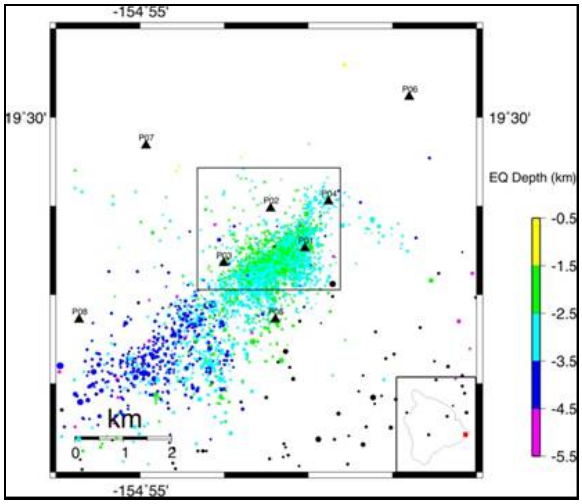

Figure 3: Map view of Puna seismic array stations and earthquakes. Black triangles are seismic stations. Earthquake locations are marked by dots colored according to depth. The size of the dots indicates the magnitude, ranging from M-0.2 to M2.0.

The Magnitude frequency distribution is usually described by the "B-value" based on the Gutenberg-Richter relationship:

$$\text{Log10}(N) = A - B*M$$

where N = number of events with Magnitude = M and B = slope of the distribution

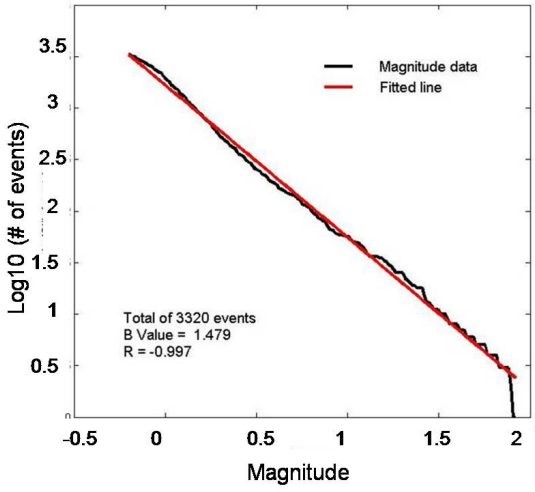

Figure 4: Plot of the number of earthquakes of a given magnitude according to the Gutenberg-Richter relationship. The slope of the plot represents the B-value, 1.48. The value of R = -0.997.

Figure 4 shows the B-value plot for all events -0.2 < Mag < 2.0 located within 5 km from the center of the detailed target zone with B-value = 1.48. The increase in slope at magnitude below 0.5 indicates that there is an increase in the number of events smaller than M0.5; 95% are of magnitude <0.5. This may be attributed to reinjection of geothermal fluid. Without this jump in the number of smaller events, the B-value is 1.3.

Seismic moments for the events were computed using the spectral method of Andrews (1986). Magnitudes were calibrated with events also detected by the Hawaiian Volcano Observatory (HVO). The lowest useable detection threshold for the PGV network is M-0.2.

4. SHEAR WAVE SPLITTING

Shear wave splits were picked automatically after the S-waves had been identified by hand. Figure 5 shows an example of a shear wave split before and following rotation.

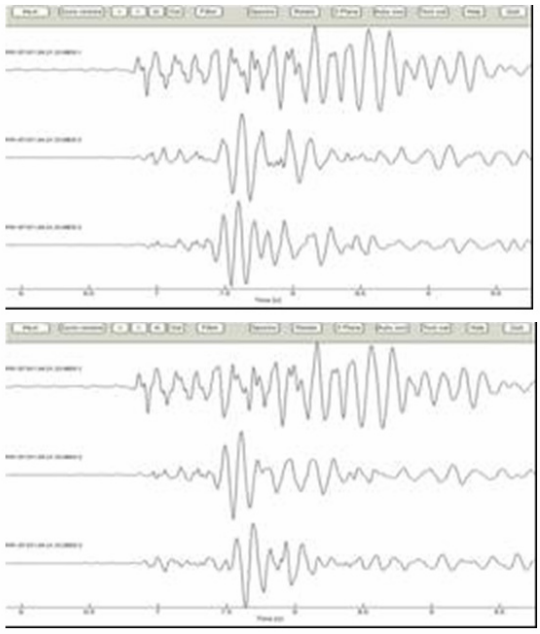

Figure 5: The upper diagram shoes the original seismogram, with no shear wave splitting identifiable. The lower diagram shows the seismogram after 56° rotation. Shear wave splitting is visible.

The dominant fracture orientation is consistent with the Kilauea East Rift Zone, i.e. trending NE (Figure 6). Rose diagrams indicate the dominant direction of fast shear-wave motion, which is generally SW-NE at the geothermal field. The slight variation of stations P4 and P5 from the general trend can be attributed to errors in station orientations derived from local seismicity. A lack of earthquakes to the northeast of the field prevented processing of shear wave splits at station P06, so it is not clear whether the northward fracture orientation continues. At P01, immediately above the largest concentration of earthquakes, there was a secondary orientation of fast shear-waves, trending W-E. This indication of a secondary fracture system is consistent with results we got from double difference relocations.

The individual fast shear wave orientations at five stations are portrayed in Figure 7, a polar coordinate projection. Each line is one observation, showing the azimuth and incident angle of the hypocenter to the projected half space. This figure shows the level of complexity of the fracture

system, where within a limited area fractures may be oriented in several different directions. The trend of the rift zone is clear, as are orientations in an E-W direction.

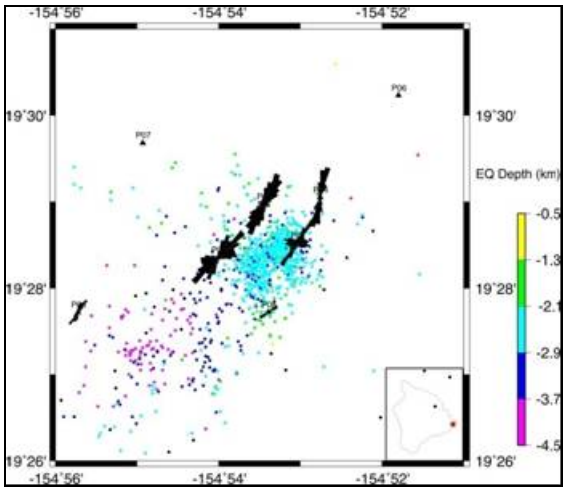

Figure 6: Rose diagrams indicating the fast shear wave polarization directions. Each bin is 5 degrees wide. The length of the bin reflects the number of shear wave splits in the bin. A total of 1500 shear wave splitting observations were made, most of them by stations close to the center of the earthquake cluster. Black triangles are seismic stations. Earthquake locations are marked by dots colored according to depth. The size of the dots indicates the magnitude, ranging from M-0.2 to M2.0.

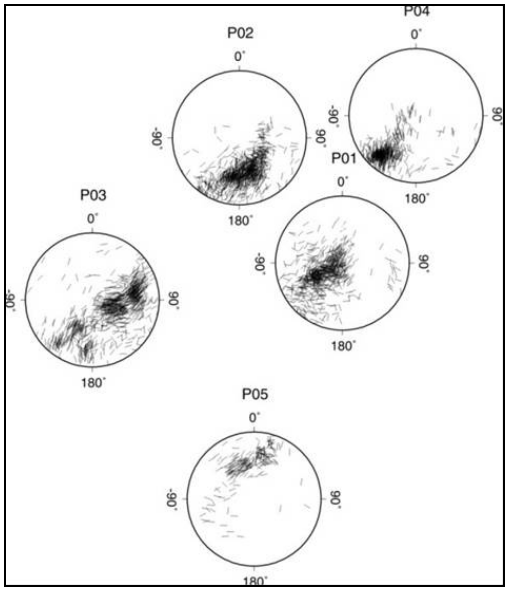

Figure 7: Polar coordinate projection (azimuth and angle) of shear wave splitting polarization. Each circle represents all shear wave splitting observations for one station. The circumference of each circle represents a 45° incident angle from the vertical. Azimuth marks the direction toward the hypocenter. The location of each line represents the azimuth and the incident angle of one shear wave splitting observation. The orientation of each line is the direction of the fast shear wave polarization for that observation. Stations P01, P02, P03, P04, and P05 are plotted in the correct geographical location.

5. DOUBLE DIFFERENCE RELOCATION

All of the earthquakes detected over the recording period were relocated using the double difference algorithm of Waldhauser (2001). Currently catalog-type data is used; it is on-going work to develop the correlation data and thus improve the current result. The absolute location of the earthquake cluster has not been adjusted, so this data set can be considered an indication of structural features rather than exact fracture locations. A comparison between the HYPOINVERSE-2000 and the double difference locations (Figure 7, following text) shows improvement in resolution.

Two broad types of patterns can be identified in the earthquake locations: Rift parallel and rift perpendicular. The dominant rift parallel structures trend in the same NE direction as those of the Kilauea rift zone (Figure 8). The secondary rift perpendicular structures are observed throughout the study area but are most strongly observable in the main body of the cluster and in the projected cross section figure (8D).

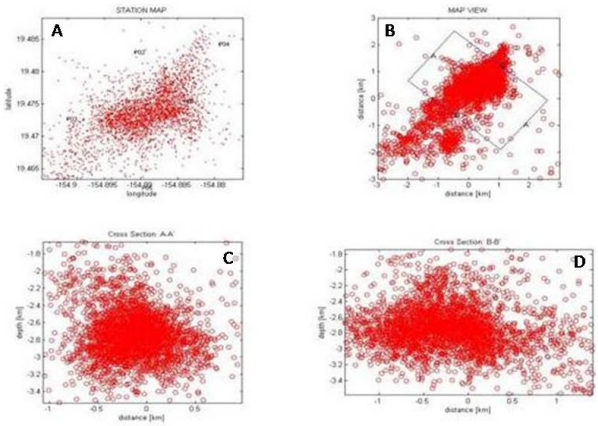

Figure 8: A, B, C, D. Map and Cross section views of events that have been double difference relocated. Figures (8A) and (8B) are both map views with 9B showing a detailed view of the area. Figure (9B) shows the area used to generate the projected cross sections in figures (8C) and (8D).

6. 3-D SEISMIC TOMOGRAPHY

Tomographic inversion followed the method described in Shalev and Lees (2004) and Lees and Shalev (1992). The preliminary velocity model was based on earthquake locations from the Hawaiian Volcano Observatory. This model was iteratively revised using the earthquakes from the current data set. Earthquakes were located and iteratively relocated in conjunction with the velocity model.

For the 3D inversion, events were used that were recorded at all eight network stations. The volume used was 2 km x 2 km x 4 km, centered at 19° 28’ 42.3N, 154° 53’ 17.6W. The volume extended from 200m above sea level to a depth of 4 km. The volume was parameterized with a grid of constant-slowness cubic cells with sides of 100 m.

Figure 9 shows the number of rays that passed through cubic volumes within the target area. The ray coverage was consistently best in the central to southern areas of the target, with the most hits at 2.5 km depth.

Vp is slower than average under the central geothermal field at 1.5 and 2 km depth; at 2.5 km and 3 km depth Vp is exceptionally fast (Figure 10).

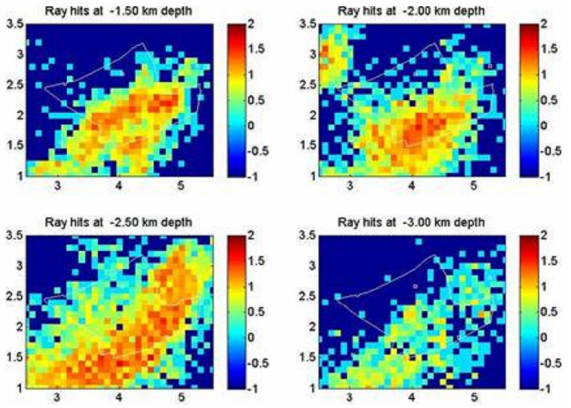

Figure 9: Hit-count map of the target zone. Images are horizontal slices at depths of 1.5, 2.0, 2.5, and 3.0 km. Colors indicate log10 number of rays that pass through each 100 m x 100 m x 100 m volume. The thin line within each map marks the PGV lease.

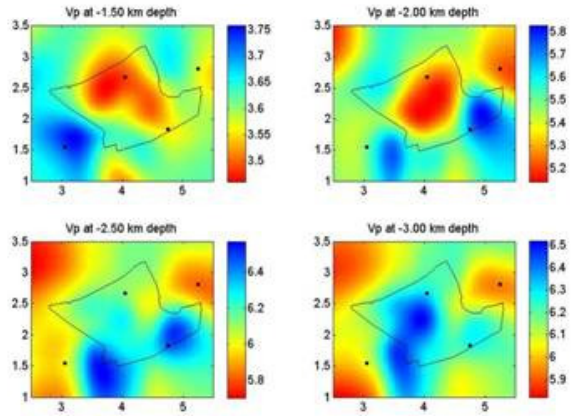

Figure 10: The 3-D tomographic inversion for P-wave velocity presents data in horizontal slices at 1.5, 2, 2.5, and 3 km depth. The figures show Vp perturbation, the change from the average velocity at each depth. Reds represent slower velocities and blues represent faster velocities.

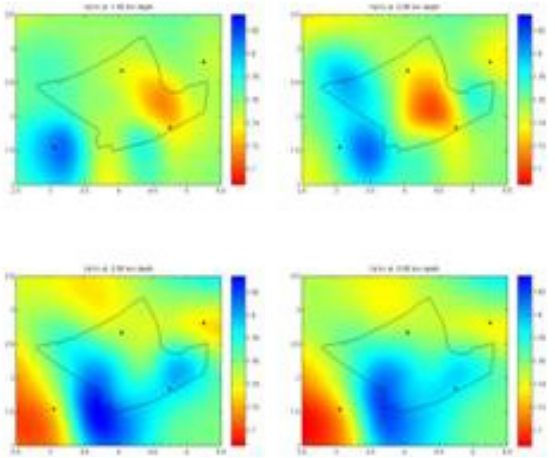

Figure 11: The 3-D tomographic inversion for Vp/Vs. Horizontal slices are at 1.5, 2, 2.5, and 3 km depth, represent slower ratios and blues represent higher ratios.

Figure 11 shows the Vp/Vs inversion. At 1.5 and 2km depth, Vp/Vs is slower than the average for the depth to the east and faster to the west. At 2.5 and 3km depth, Vp/Vs is faster to the south. Because of the fast P-wave velocities at 2.5-3 km depth, it is likely that the high Vp/Vs values are more strongly affected by P-wave than S-wave velocity.

6. DISCUSSION

Hydrothermal areas commonly occur in zones of fault propagation and interaction (e.g. Curewitz and Karson, 1997 and references therein). The Puna geothermal area is located in a "jog" between the ends of two rift segments separated by approximately 1.5 km; this area may be a transfer zone, where the interaction between fault tips has caused increased fracturing and permeability. The dominant structure underlying the system consists of normal faulting, with northeasterly strike, parallel to the Kilauea East Rift Zone and dipping to the south. By contrast, our double difference results are consistent with the shear wave splitting results and indicate cross-cutting fractures approximately orthogonal to the NE trend. At Krafla, Iceland, a magnetotelluric survey (Onacha, 2007) and shear wave splitting (Tang, 2008) also have observed fractures orthogonal to the dominant rift/normal faulting direction.

Secondary fractures approximately orthogonal to the dominant normal fault strike have been addressed in two similar models, Hill (1977) and Rowland and Sibson (2004). Hill (1977) describes the formation of dikes and conjugate faults as related to earthquake swarms from dike intrusions. Rock permeability increases as dikes develop and open in the σ_2 direction. Rowland and Sibson (2004) describe a similar model to explain permeability in the rift system at Taupo Volcanic Zone, New Zealand. As in any system, normal faulting at the Kilauea LERZ must be accompanied by secondary movement to accommodate stress.

The tomographic results showing high P-wave velocity at ~2 km corresponds to a region just below where Puna Geothermal Ventures drilled into a body of active dacitic melt. The melt itself appears to be too small to be seen with the resolution of our array; future work includes analyzing for a melt-related S-wave shadow. Since P-wave velocities increase underneath the melt body, we hypothesize that the high-velocity body is an intruded gabbro, an intrusive rock of basaltic composition but with higher crystallinities and higher seismic velocities (Vp = ~6.7 km/sec). The presence of the magma body is an astonishing scientific opportunity, and proposals are being submitted to the US National Science Foundation and Department of Energy to try to obtain funding for further drilling and research.

7. CONCLUSIONS

1. In the Puna geothermal field, the dominant pattern of seismicity aligns parallel to the Kilauea Lower East Rift Zone. The majority of earthquakes occurs at 2-3 km depth, possibly associated with activity at the geothermal production plant.

2. Secondary fractures approximately orthogonal to the primary faulting are indicated by shear wave splitting analysis and double difference earthquake location. Further work to improve double difference locations includes correlating waveforms and calculating absolute locations of fractures. In addition, we are analyzing many small, linear features chronologically by video. With step by step hypocenter chronology, we can isolate swarms and see the pattern of features along which they occur.

3. 3-D tomography indicates the presence of a high-velocity zone under the central geothermal field. The zone underlies a dacitic melt body at ~2 km depth; it is possibly a gabbroic intrusion that was the source of the melt.

REFERENCES

Chiarabba, C. and Moretti, M.: An insight into the unrest phenomena at the Campi Flegrei caldera from Vp and Vp/Vs tomography, *Terra Nova*, 18, 6, 373-379, (2006)

Clarke, D., Townend, J., Savage, M.K., and Bannister, S.: Seismicity in the Rotorua and Kawerau geothermal systems, Taupo Volcanic Zone, New Zealand, based on improved velocity models and cross-correlation measurements, *Journal of Volcanology and Geothermal Research*, 180, 50-66, (2009)

Crampin, S.: A review of wave motion in anisotropic and cracked elastic-media, *Wave Motion*, 3, 343-391, (1981)

Crampin, S. and Peacock, S.: A review of shear-wave splitting in the compliant crack-critical anisotropic Earth, *Wave Motion*, 41, 59-77, (2005)

De Matteis, R., Vanorio, T., Zollo, A., Ciuffi, S., Fiordelisi, A., and Spinelli, E.: Three-dimensional tomography and rock properties of the Larderello-Travale geothermal area, Italy, *Physics of the Earth and Planetary Interiors*, 168, 37-48, (2008)

Gunasekera, R.C., Foulger, G.R., and Julian, B.R.: Reservoir depletion at the Geoysers geothermal area, California, shown by four-dimensional seismic tomography, *Journal of Geophysical Research*, 108 (B3), 2134, doi:10.1029/2001JB000638, (2003)

Gutenberg, B. and Richter, C.F.: *Seismicity of the Earth and Associated Phenomena*, 2nd ed., Princeton, N.J.: Princeton University Press, 17-19, (1954)

Klein, F.W.: Hypocenter location program HYPOINVERSE-2000, *U.S. Geological Survey Open File Report 02-171* (2002)

Lees, J.M.: Seismic tomography of magmatic systems, *Journal of Volcanology and Geothermal Research*, 167, 37-56, (2007)

Lees, J.M. and Shalev, E.: On the stability of P-wave tomography at Loma Prieta: A comparison of parameterizations, linear and non-linear inversions, *Bulletin of the Seismological Society of America*, 82, 4, 1821-1839, (1992)

Lippitsch, R., White, R.S., and Soosalu, H.: Precise hypocenter relocation of microearthquakes in a high-temperature geothermal field: the Torfajokull central volcano, Iceland, *Geophysical Journal International*, 160, 370-387, (2005)

Lou, M., Shalev, E., and Malin, P.E.: Shear-wave splitting and fracture alignments at the Northwest Geysers, California, *Geophysical Research Letters*, 24, 1895-1898, (1997)

Marsh, B., Teplow, W., Reagan, M., and Sims, K.: Puna Dacite: Likely Temperature, Viscosity, origin, size, and parent body nature, *EOS Transactions AGU*, 89(53), Fall Meeting Supplement, Abstract V23A-2130, (2008)

Moore, R.B. and Trusdell, F.A.: Geologic map of the Lower East Rift Zone of Kilauea Volcano, Hawaii, U.S. Geological Survey Miscellaneous investigations series, map I-2225, (1991)

Onacha, S.A.: PhD Dissertation Duke University (2007).

Parfitt, E.A. and Peacock, D.C.P.: Faulting in the South Flank of Kilauea Volcano, Hawaii, *Journal of Volcanology and Geothermal Research*, 106, 265-284, (2001)

Prejean, S., Ellsworth, W., Zoback, M., and Waldhauser, F.: Fault structure and kinematics of the Long Valley Caldera region, California, revealed by high-accuracy earthquake hypocenters and focal mechanism stress inversions, *Journal of Geophysical Research*, 107, B12, 2355, doi:10.1029/2001JB001168, (2002)

Prejean, S., Stork, A., Ellsworth, W., Hill, D., and Julian, B.: High precision earthquake locations reveal seismogenic structure beneath Mammoth Mountain, California, *Geophysical Research Letters*, 30, 24, 2247, doi:10.1029/2003GL018334, (2003)

Rial, J.A., Elkibbi, M., Yang, M.: Shear-wave splitting as a tool for the characterization of geothermal fractured reservoirs: lessons learned, *Geothermics*, 34, 365-385, (2005)

Shalev, E. and Lees, J.M.: Three dimensional tomographic analysis of the Loma Prieta region. In: *The Loma Prieta, California, Earthquake of October 17, 1989 - Geologic Setting and Crustal Structure*, R.E. Wells (Editor), USGS Professional Paper 1550-E, U.S. Geological Survey, Reston, VA, 127-142, (2004)

Tang, C., Rial, J.A., and Lees, J.M.: Seismic imaging of the geothermal field at Krafla, Iceland using shear-wave splitting, *Journal of Volcanology and Geothermal Research*, 315-324, (2008)

Teplow, W., Marsh, B., Hulen, J., Spielman, P., Kaleikini, M., Fitch, D.C. and Rickard, W.: Dacite melt at the Puna Geothermal Venture Wellfield, Big Island of Hawaii, *EOS Transactions AGU*, 89(53), Fall Meeting Supplement, Abstract V23A-2129, (2008)

Trusdell, F.A., Novak, E., Evans, S.R.: Core lithology State of Hawaii scientific observation hole 4, Kilauea Volcano, Hawaii, U.S. Geological Survey Open-file report 92-586 (1993)

Waldhauser, F.: hypoDD: A program to compute double-difference hypocenter locations, *U.S. Geological Survey Open File Report 01-113*, 25pp, (2001)

Waldhauser, F, and Ellsworth, W.L., A double-difference earthquake location algorithm: method and application to the Northern Hayward Fault, California, *Bulletin of the Seismological Society of America*, 90, 1353-1368, (2000)